

Quantitative explanation of the magnetic resonance peak in high-temperature superconductors: Evidence for an extended s-wave pairing symmetry

Guo-meng Zhao

Department of Physics and Astronomy, California State University at Los Angeles, Los Angeles, CA 90032, USA

The microscopic pairing mechanism responsible for high-temperature superconductivity in copper-based perovskite oxides is still a subject of intense debate despite tremendous experimental and theoretical efforts for over 15 years. The debate has centered around the role of antiferromagnetic spin fluctuations in high-temperature superconductivity and the symmetry of superconducting condensate (order parameter). Extensive inelastic neutron scattering experiments have accumulated a great deal of important data that should be sufficient to address these central issues. Of particular interest is the magnetic resonance peak that has been observed in double-layer cuprate superconductors such as $\text{YBa}_2\text{Cu}_3\text{O}_{7-y}$ [1,6] and $\text{Bi}_2\text{Sr}_2\text{CaCu}_2\text{O}_{8+y}$ [7,8], and in a single-layer compound $\text{Tl}_2\text{Ba}_2\text{CuO}_{6+y}$ [9]. A number of theoretical models [10-13] have been proposed to explain the magnetic resonance peak, pointing to a magnetic fluctuation mediated d-wave pairing mechanism. Here we identify several important features in the neutron scattering data of cuprates, which can definitively rule out d-wave and isotropic s-wave order parameters. We further show that the neutron data are in quantitative agreement with an order parameter that has an extended s-wave (A_{1g}) symmetry [14,15] and opposite signs in the bonding and antibonding electron bands formed within the Cu_2O_4 bilayers [16]. The identification of the extended s-wave pairing symmetry rules out the important role of magnetic excitations in superconductivity and provides strong support to a charge fluctuation mediated pairing mechanism [17,18].

Despite their electrostatic repulsion, the phenomenon of superconductivity involves the pairing of electrons into Cooper pairs [19]. These Cooper pairs obey a certain internal symmetry which reflects the underlying pairing mechanism. It is well known that the conventional low- T_c superconductors (e.g., Pb, Al, and Nb) possess an s-wave symmetry that reflects the phonon mediated electron-electron pairing [19]. On the other hand, the internal structure of the Cooper pairs in the high- T_c cuprate superconductors has been a topic of intense debate for over fifteen years. Three pairing symmetry contenders have been isotropic s-wave, d-wave and extended s-wave, as depicted in Fig. 1. Both d-wave and extended s-wave have line nodes and change signs when a node is crossed. Experiments to test these symmetries sometimes involve surface sensitive artifacts which may not

probe the intrinsic bulk pairing symmetry. By virtue of its phase, angle and bulk-sensitive nature, inelastic neutron scattering (INS) is one of the most robust experimental probes of the pairing symmetry. In this paper we devote special attention to the INS data and briefly reference or comment on other probes to definitively argue for extended s-wave symmetry and against both isotropic s- and d-wave symmetries.

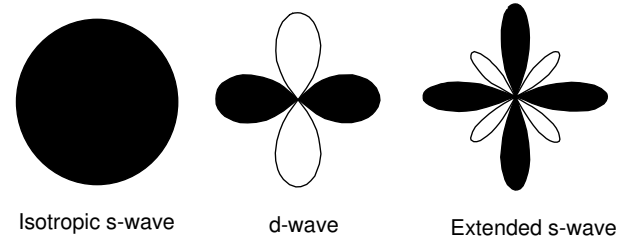


FIG. 1. Three allowed pairing symmetries appropriate for CuO_2 planes in the high- T_c superconductors. Both d-wave and extended s-wave have line nodes and change signs when a node is crossed.

The magnetic resonance peak observed in optimally doped and overdoped double-layer compounds $\text{YBa}_2\text{Cu}_3\text{O}_y$ (YBCO) [1,5] and $\text{Bi}_2\text{Sr}_2\text{CaCu}_2\text{O}_{8+y}$ (BSCCO) [7,8] is a sharp collective mode that occurs at an energy of 38-43 meV and at the two-dimensional wavevector $\vec{Q}_{AF} = (\pi, \pi)$, where a is the nearest-neighbor Cu-Cu distance. Fig. 2a shows the imaginary part of dynamic spin susceptibility as a function of excitation energy for an optimally doped double-layer compound $\text{YBa}_2\text{Cu}_3\text{O}_{6.92}$. The figure is reproduced from Ref. [5]. There are several striking features in the data: (a) The resonance peak at $E_r = 41$ meV appears below T_c and this resonance peak intensity in the superconducting state $I^S(E_r)$ is larger than the normal-state intensity $I^N(E_r)$ by a factor of about 3.6, i.e., $I^S(E_r)/I^N(E_r) = 3.6$; (b) A spin gap feature is seen below T_c and there is a small shoulder that occurs at an energy slightly above the spin gap energy $E_g = 32$ meV. Fig. 2b shows a q_{\parallel} -scan at $E = 40$ meV in $\text{YBa}_2\text{Cu}_3\text{O}_{6.92}$ displaying a modulation typical of odd excitation. The figure is reproduced from Ref. [4]. From Fig. 2b, we find feature (c): The inter-layer scattering intensity within the Cu_2O_4 bilayers (odd channel) is larger than the intralayer scattering intensity (even channel) by a factor of about 5 (Ref. [4]), i.e., $I_{\text{odd}}^S(E) = I_{\text{even}}^S(E) = 5$ for $E = 40$ meV. From the neutron studies on different double-layer compounds with different

ent doping levels, one identifies feature (d): The resonance energy E_r does not increase with doping in the overdoped range but is proportional to T_c as $E_r = k_B T_c = 5.2$ in both underdoped and overdoped ranges [8].

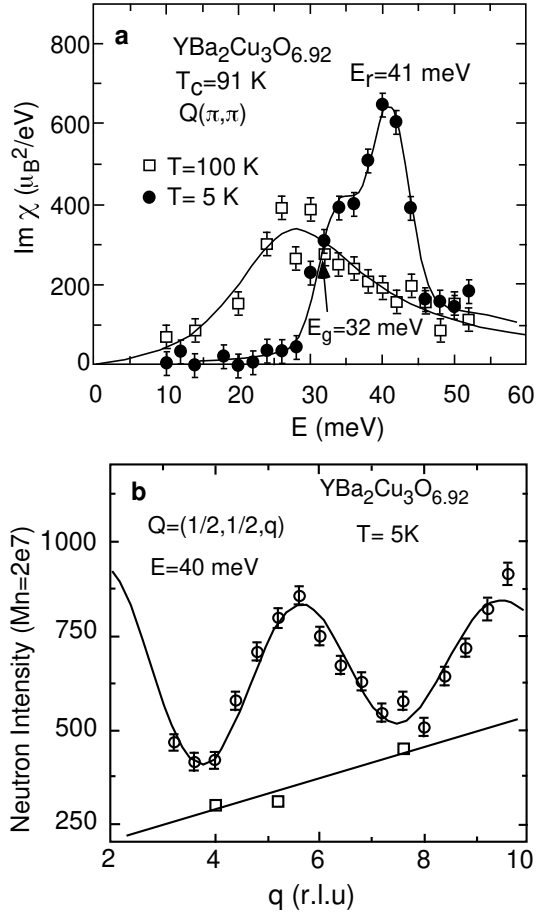


FIG. 2. a) The imaginary part of dynamic spin susceptibility as a function of excitation energy for $\text{YBa}_2\text{Cu}_3\text{O}_{6.92}$ in the normal and superconducting states. The figure was reproduced from Ref. [5]. b) q_1 -scan at $E = 40$ meV in $\text{YBa}_2\text{Cu}_3\text{O}_{6.92}$ displaying a modulation typical of odd excitation. The figure was reproduced from Ref. [4]. The background (lower line and open squares) was obtained from q -scans across the magnetic line. The upper solid curve is a fit to $a + bF^2(Q) \sin^2(zq_1)$, where $F(Q)$ is the Cu magnetic form factor. The modulation is not complete as even excitations are sizable at $q_1 = 3.5, 7$ but with a magnitude 5 times smaller [4].

On the other hand, the neutron data for an optimally doped single-layer compound $\text{Tl}_2\text{Ba}_2\text{CuO}_{6+y}$ (T-2201) are different from those for double-layer compounds. For the single-layer T-2201, we show in Fig. 3a the differential spectrum of the neutron intensities at $T = 27$ K ($< T_c$) and $T = 99$ K ($> T_c$), at a wavevector of $Q = (0.5, 0.5, 12.25)$. The figure is reproduced from Ref. [9]. Although a sharp peak feature is clearly seen at $E_r = 47.5$ meV, it is remarkable that the peak intensity in the supercon-

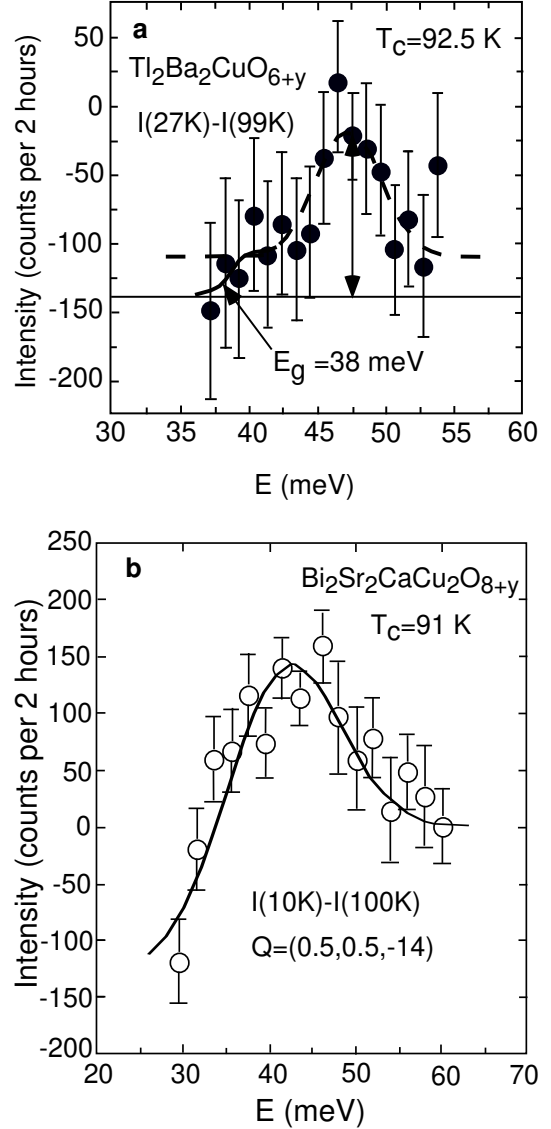


FIG. 3. a) The differential spectrum of the neutron intensities of single-layer T-2201 crystals (with a total volume of 0.11 cm^3) at $T = 27$ K ($< T_c$) and $T = 99$ K ($> T_c$), and at wavevector $Q = (0.5, 0.5, 12.25)$. The figure is reproduced from Ref. [9]. The dashed curve is the original fit in Ref. [9] while the solid curve below 40 meV is a new fit, which is used to deduce the magnitude of the spin gap. The peak intensity of a Q scan along $Q = (q, q, 12.25)$ at $E = 47.5$ meV (see Fig. 4 of Ref. [9]) is indicated by a vertical arrow. The nonmagnetic background intensity in the E scan is assumed to be the same as that in the Q scan and is indicated by the horizontal solid line. b) The differential spectrum of the neutron intensities of optimally doped BSCCO crystals (with a total volume of 0.06 cm^3) at $T = 10$ K ($< T_c$) and $T = 100$ K ($> T_c$), and at wavevector $Q = (0.5, 0.5, -14)$. The figure is reproduced from Ref. [7]. It is worth noting that if the magnetic resonance peak in BSCCO were as sharp as that in T-2201, the peak intensity in BSCCO would increase by a factor of about 2.5.

ducting state is less than the magnetic neutron intensity in the normal state. From the peak intensity of a Q scan

along $Q = (q, q, 12.25)$ at $E = 47.5$ meV (see Fig. 4 of Ref. [9]), the nonmagnetic background intensity is deduced (as indicated by the horizontal solid line) on the assumption that the nonmagnetic background intensity in the E scan is the same as that in the Q scan. With this knowledge of the nonmagnetic background contribution, we find that the resonance peak intensity $I^S(E_r)$ for the single-layer Tl-2201 is slightly lower than the normal-state intensity $I^N(E_r)$, i.e., $I^S(E_r)/I^N(E_r) = 0.87$. This is in sharp contrast with the above result for the double-layer compound $YBa_2Cu_3O_{6.92}$ where we found $I^S(E_r)/I^N(E_r) = 3.6$. Thus we identify feature (e) as $I^S(E_r)/I^N(E_r) < 1$ for single-layer compounds.

We would like to mention that feature (e) identified for the single-layer Tl-2201 is valid only if the nonmagnetic background has a negligible temperature dependence below 100 K. It is known that nuclear contributions predominantly due to unresolved single phonon events constitute the main part of the neutron signal [3]. Any nuclear contributions are only expected to obey the following standard temperature dependence, $1 = \exp(-E/k_B T)$ (see discussions in Ref. [3]). In the energy range of interest ($E > 40$ meV), this temperature dependence factor is close to unity and nearly independent of temperature for $T < 150$ K. Indeed, neutron intensities of both YBCO [3] and BSCCO [7,8] show a negligible temperature dependence for $T_c < T < 150$ K. For $E = E_r = 47.5$ meV in Tl-2201, this factor decreases by 0.38% when the temperature goes from 99 K to 27 K. If we take the nonmagnetic background of 2500 counts per two hours [9], the nonmagnetic background decreases by 10 counts per two hours when the temperature goes from 99 K to 27 K, and by 53 counts per two hours when the temperature goes from 150 K to 99 K. The variation of the nonmagnetic background at $E = 47.5$ meV below 100 K is negligibly small compared with the magnetic resonance intensity (~ 130 counts per two hours). Therefore, feature (e) identified for the single-layer Tl-2201 is well justified.

In order to further justify feature (e), we compare the neutron data for double-layer BSCCO [7,8] with that for the optimally doped single-layer Tl-2201 (Ref. [9]). From the data, we see that the signal-to-background ratio is about 8% for the optimally doped Tl-2201 (Ref. [9]), about 12% for the optimally doped BSCCO [7] and about 6% for the overdoped BSCCO [8]. The ratio does not show a significant difference, suggesting that the insignificant difference in the nonmagnetic backgrounds in these experiments should not be the cause of the pronounced difference in their differential spectra shown in Fig. 3a and Fig. 3b. Further, even with a very significant difference in the nonmagnetic backgrounds in the experiments on YBCO and BSCCO, the differential spectra of the two double-layer compounds are similar (see Refs. [3] and [7]). Therefore, the pronounced difference in the dif-

ferential spectra of Tl-2201 and BSCCO is due to the fact that $I^S(E_r)/I^N(E_r) \gg 1$ for the double-layer BSCCO while $I^S(E_r)/I^N(E_r) < 1$ for the single-layer Tl-2201.

Several theoretical models have been proposed to explain the magnetic resonance peak. In a more exotic approach [10], the neutron data are interpreted in terms of a collective mode in the particle-particle channel whose quantum numbers are spin 1 and charge 2 (like triplet bipolarons [20]). This model predicts that the resonance peak energy E_r is proportional to the doping level p . Other theories based on spin-fermion interactions or t-J model also show that E_r increases monotonically with increasing p [11-13]. All these models are in disagreement with feature (d): E_r does not increase with increasing p in the overdoped range but is proportional to T_c as $E_r = k_B T_c = 5.2$ (Ref. [8]). Further, all d-wave models [10-13] predict that $I^S(E_r)/I^N(E_r) \gg 1$ even for single-layer compounds, which definitively contradicts feature (e): $I^S(E_r)/I^N(E_r) < 1$ for the single-layer Tl-2201 (see Fig. 3a).

Alternatively, feature (d) is consistent with a simple particle-hole excitation across the superconducting gap within an itinerant magnetism model. This is because the particle-hole excitation energy increases with the superconducting gap which in turn should be proportional to T_c at least in the overdoped range. This itinerant magnetism model is also supported by very recent Fourier transform scanning tunnelling spectroscopic (FT-STs) studies on a nearly optimally doped BSCCO [21], which show that the quasiparticles in the superconducting state exhibit particle-hole mixing similar to that of conventional Fermi-liquid superconductors. These FT-STs results thus lead us to believe that the itinerant magnetism approach is suitable for optimally doped and overdoped cuprates. Here we quantitatively explain all these neutron data [9] in terms of an order parameter (OP) that has an extended s-wave symmetry [14,15] and opposite signs in the bonding and antibonding electron bands formed within the Cu_2O_4 bilayers [16]. In our model, the neutron resonance peak is due to excitations of electrons from the extended saddle points below the Fermi level to the superconducting gap edge above the Fermi level.

Within the itinerant magnetism model, neutron scattering intensity at a wavevector q and an energy E is proportional to the imaginary part of the dynamic electron spin susceptibility, $\chi''(q; E)$. Qualitatively, with the neglect of the Bardeen-Cooper-Schrieffer (BCS) coherence factor, the bare imaginary part of spin susceptibility, $\chi''(q; E)_P$, is proportional to the joint density of states $A(q; E) = \frac{1}{\pi} \int_{\mathbf{k}} \delta(E - E_{\mathbf{k}+q} - E_{\mathbf{k}})$, where $E_{\mathbf{k}} = \frac{\hbar^2 k_x^2}{2m} + \frac{\hbar^2 k_y^2}{2m}$ is the quasiparticle dispersion law below T_c , $\epsilon_{\mathbf{k}}$ is the electronic band dispersion, and $\Delta_{\mathbf{k}}$ is the order parameter [16]. The two-particle energy $E_2(\mathbf{k}; q) = E_{\mathbf{k}+q} + E_{\mathbf{k}}$ has a minimum and several saddle points for a fixed q . The minimum defines the threshold energy, or spin gap

energy E_g , which is achieved at vector \mathbf{k} and $\mathbf{k} + \mathbf{q}$ such that both \mathbf{k} and $\mathbf{k} + \mathbf{q}$ belong to the Fermi surface and thus $E_g = 2 \epsilon_{\mathbf{k}}$ (Ref. [16]).

The joint density of states has a step at E_g and divergences at the extended saddle points [16]. The divergent peak in $\rho(E; \mathbf{q}; !)$ occurs because of transitions between the occupied states located in the extended saddle points below E_F and empty quasiparticle states at the superconducting gap edge above E_F . The saddle points produce Van Hove singularities in the quasiparticle density of states in the superconducting state at an energy of $\epsilon_{\mathbf{k}} = \frac{(\mathbf{v}^H)^2}{2\mathbf{k}}$ and the superconducting condensate creates a sharp coherence peak in the quasiparticle density of states at the gap edge. Thus, the divergence in the joint density of states in the superconducting state is then located at the energy $E = \epsilon_{\mathbf{k}+\mathbf{q}} + \frac{(\mathbf{v}^H)^2}{2\mathbf{k}}$. This simple expression for E has been verified by numerical calculations in the case of an isotropic s-wave order parameter [16].

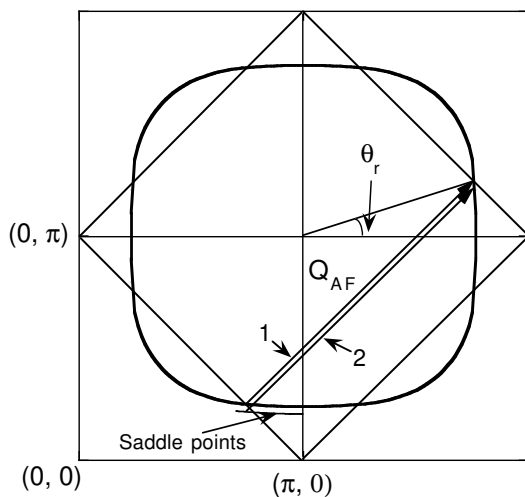


FIG. 4. The Fermi surface for a slightly underdoped BSCCO with $T_c = 88$ K. This Fermi-surface is extrapolated from part of the Fermi surface determined by ARPES [22] using symmetry arguments. Arrow 1 indicates electron transitions from the occupied states in the superconducting gap edge below E_F to empty quasiparticle states at the gap edge above E_F . Arrow 2 marks electron transitions from the occupied states located in the extended saddle points below E_F to empty quasiparticle states in the superconducting gap edge above E_F .

In Fig. 4, we plot the Fermi surface for a slightly underdoped BSCCO, which is inferred by extending part of the Fermi surface determined by angle-resolved photoemission spectroscopy (ARPES) [22]. There are extended saddle points that are located near $(\pi, 0)$ and $(0, \pi)$, as shown by ARPES [23]. A solid line in Fig. 4 represents a segment of the extended saddle points very close to the Fermi surface. Other portions of the saddle points

[e.g., along the line from $(0, 0)$ to $(\pi, 0)$] are significantly away from the Fermi surface [23] and not shown in the figure. If we only consider the magnetic excitations at a fixed wavevector that corresponds to the antiferromagnetic wavevector Q_{AF} , only four electron wavevectors at the Fermi surface are connected by Q_{AF} as indicated by arrow 1 in Fig. 4. Each of these vectors forms an angle of θ_r with respect to the Cu-O bonding direction. The electron transitions from the occupied states located at the extended saddle points below E_F to empty quasiparticle states at the superconducting gap edge above E_F are indicated by arrow 2. Because the quasiparticle densities of states at the gap edge and the saddle points are divergent at zero temperature, such transitions will produce a sharp resonance peak at $E_r = \epsilon_{\mathbf{k}+Q_{AF}} + \frac{(\mathbf{v}^H)^2}{2\mathbf{k}}$.

In terms of θ_r , both $E_g(Q_{AF})$ and $E_r(Q_{AF})$ can be rewritten as

$$E_g(Q_{AF}) = 2 \epsilon_{\theta_r} \quad (1)$$

and

$$E_r(Q_{AF}) = \epsilon_{\theta_r} + \frac{\mathbf{q}^2}{[(\theta_r)^2 + (\mathbf{v}^H)^2]^{3/2}} \quad (2)$$

Here $\frac{\mathbf{q}^2}{[(\theta_r)^2 + (\mathbf{v}^H)^2]^{3/2}}$ is the energy of a saddle point below the Fermi level along the θ_r direction. One should note that Eq. 2 is valid only if the saddle points are very close to the Fermi surface, as is the case.

This bare electron picture can explain the neutron resonance feature in the energy scan with a fixed Q_{AF} (see above). However, it cannot explain the neutron resonance feature in the Q scan at a fixed resonance energy because the observed peak is sharply located at Q_{AF} while this simple model predicts the existence of peaks in other values of q if the order parameter is an isotropic s-wave. For an anisotropic s-wave, the peaks exist for other values of q but with different energies.

In order to understand the Q scan at a fixed resonance energy, one needs to consider the antiferromagnetic correlation between conduction electrons, which has been clearly seen in nuclear magnetic resonance studies [24]. In the presence of antiferromagnetic correlation, the bare spin susceptibility is renormalized in a random phase approximation [25]. Since the antiferromagnetic interaction between the nearest neighbors produces a peak at Q_{AF} , the renormalized spin susceptibility has a sharp maximum at Q_{AF} . In other words, because of the antiferromagnetic correlation, the dynamic spin susceptibility is greatly enhanced only near Q_{AF} so that the susceptibility for other wavevectors is negligibly small compared

with the one near Q_{AF} . In light of this picture, one expects that the neutron intensities at fixed Q_{AF} in both normal and superconducting states should increase with decreasing doping because the antiferromagnetic correlation also increases with decreasing doping. This is in agreement with experiment [4].

We now consider the BCS coherence factor that has been ignored in the above discussions. The BCS coherence factor is given by [26]:

$$\langle \sigma_j | \sigma_k \rangle = \frac{1}{2} \left(1 + \frac{\xi_{k+q} + \xi_k}{E_k E_{k+q}} \right); \quad (3)$$

For $k \ll k_F$ and $k+q \ll k_F$, the BCS coherence factor is close to 1 when $k+q$ and k have opposite signs, but is close to zero when $k+q$ and k have the same sign. However, the coherence factor is not negligible for $k \sim k_F$ and $k+q = 0$ even if $k+q$ and k have the same sign. More specially, for excitation energies close to the resonance energy and for the excitations at Q_{AF} , the dominant contribution to the neutron intensity is the electron excitations from the states near the saddle points below the Fermi level to the superconducting gap edge above the Fermi level. This is because the quasiparticle density of states near the gap edge is divergent at zero temperature and because the density of states near the saddle points is large. Then the final states for electron excitations are limited to the states with $\xi_{k+Q_{AF}} = 0$. By setting $\xi_{k+Q_{AF}} = 0$ in Eq. 3, we find that

$$\langle \sigma_j | \sigma_k \rangle = \frac{1}{2} \left(1 + \frac{\xi_k}{E_k} \right) = \frac{1}{2} \left(1 + \frac{E_g}{2E_k} \right); \quad (4)$$

where + corresponds to the case where $\xi_{k+Q_{AF}}$ and ξ_k have opposite signs and - to the case where $\xi_{k+Q_{AF}}$ and ξ_k have the same sign. It is apparent that for $E_r \ll E_g$, $\langle \sigma_j | \sigma_k \rangle$ is close to 1 while $\langle \sigma_j | \sigma_k \rangle \approx 0$. When E_r is comparable to E_g , both $\langle \sigma_j | \sigma_k \rangle$ and $\langle \sigma_j | \sigma_k \rangle$ are finite and $\langle \sigma_j | \sigma_k \rangle \gg \langle \sigma_j | \sigma_k \rangle$. Since the neutron intensity is proportional to the BCS coherence factor, one should see the magnetic resonance peak as long as the BCS coherence factor at the resonance energy is substantial. This is always the case when $\xi_{k+Q_{AF}}$ and ξ_k have opposite signs. This is also the case when $\xi_{k+Q_{AF}}$ and ξ_k have the same sign and E_r is significantly larger than E_g .

For a single-layer compound with d-wave order parameter symmetry, $\xi_{k+Q_{AF}}$ and ξ_k have opposite signs so that $\langle \sigma_j | \sigma_k \rangle \approx 1$ and thus $I^S(E_r)/I^N(E_r) \gg 1$. Therefore, the experimental observation of $I^S(E_r)/I^N(E_r) = 0.87 < 1$ in the single-layer Tl-2201 [9] rules out the d-wave order parameter. This unique feature can also rule out the role of the magnetic resonance peak in superconductivity. This is because all the theoretical models that emphasize an important role of the magnetic resonance peak in superconductivity require $I^S(E_r)/I^N(E_r) \gg 1$, in contradiction with feature (e) which we have identified

above. Alternatively, for a single-layer compound with an s-wave symmetry, $\xi_{k+Q_{AF}}$ and ξ_k have the same sign and $\langle \sigma_j | \sigma_k \rangle < 1$. In this case, $I^S(E_r)$ could be smaller or larger than $I^N(E_r)$ depending on the value of $\langle \sigma_j | \sigma_k \rangle$ and the sharpness of the resonance. Using $E_r = 47$ meV, $E_g = 38$ meV (see Fig. 3a), and Eq. 4, we calculate $\langle \sigma_j | \sigma_k \rangle = 0.16$. The rather small value of $\langle \sigma_j | \sigma_k \rangle$ may make $I^S(E_r)/I^N(E_r) < 1$, in agreement with the experimental result [9]. Hence, only intraplane s-wave symmetry is compatible with the observed result: $I^S(E_r)/I^N(E_r) = 0.87$.

For a double-layer compound, interactions within Cu_2O_4 bilayers yield bonding and antibonding bands. Transitions between electronic states of the same type (bonding-to-bonding or antibonding-to-antibonding) and those of opposite types are characterized by even or odd symmetry, respectively, under exchange of two adjacent CuO_2 layers. As a result, the magnetic excitations between different layers correspond to odd channel excitations while the excitations within the same layer to even channel excitations [4]. If the order parameters in the bonding and antibonding bands have the same sign, the magnetic resonance intensities in both channels should be similar for either s-wave or d-wave symmetry within the same band. This is because the BCS coherence factors for both channels are the same in this case. On the other hand, if the order parameter has an s-wave symmetry and opposite signs in the bonding and antibonding electron bands, the magnetic resonance intensity in the odd channel will be much larger than that in the even channel due to the large difference in their BCS coherence factors. Therefore, only if the order parameter has an s-wave symmetry and opposite signs in the bonding and antibonding electron bands, can the observed feature (c): $I_{odd}^S = I_{even}^S = 5$ be explained within the itinerant magnetism approach.

One may argue that feature (c) would be also explained if the antiferromagnetic correlation would remain strong in optimally doped and overdoped YBCO so that the optical magnon gaps were larger than the resonance energy of 40 meV. This is apparently not the case. Neutron data for underdoped samples [27] show that the optical magnon gap is about 50 meV for $YBa_2Cu_3O_{6.5}$ and is reduced to 25 meV for $YBa_2Cu_3O_{6.7}$. This indicates that the antiferromagnetic correlation decreases rapidly with increasing doping. If we linearly extrapolate the optical magnon gap with the oxygen content, the gap will go to zero in $YBa_2Cu_3O_y$ for $y > 0.9$, implying that the itinerant magnetism approach is valid for optimally doped and overdoped cuprates. In any case, the optical magnon gaps in optimally doped and overdoped YBCO must be much smaller than the resonance energy of 40 meV. Moreover, for the underdoped $YBa_2Cu_3O_{6.7}$, the even-channel magnetic intensity in the normal state is nearly the same as the odd-channel one

for $E = 40$ meV (Ref [27]) even if the antiferromagnetic correlation in this underdoped compound remains substantial. This implies that the interlayer antiferromagnetic correlation does not influence magnetic excitations well above the optical magnon gap [27]. Since the optical magnon gaps for optimally doped and overdoped YBCO are much smaller than that for the underdoped $\text{YBa}_2\text{Cu}_3\text{O}_{6.7}$ where $I_{\text{odd}}^{\text{N}}(E) = I_{\text{even}}^{\text{N}}(E) \approx 1$ for $E \approx 40$ meV, it is natural that $I_{\text{odd}}^{\text{N}}(E) = I_{\text{even}}^{\text{N}}(E) = 1$ for $E \approx 40$ meV in optimally doped and overdoped YBCO. Thus the observed feature (c): $I_{\text{odd}}^{\text{S}}(E_r)/I_{\text{even}}^{\text{S}}(E_r) \gg 1$ for optimally doped and overdoped YBCO can only be explained by an OP that has s-wave symmetry and opposite signs in the bonding and antibonding electron bands.

Because the magnetic intensity is proportional to the BCS coherence factor, the difference in the magnetic resonance intensities in the even and odd channels is due to the difference in their BCS coherence factors that are associated with the sign of the order parameter. This simple argument leads to a relation

$$\frac{I_{\text{odd}}^{\text{S}}(E)}{I_{\text{even}}^{\text{S}}(E)} = \frac{+ (E)}{(E)} : \quad (5)$$

For the optimally doped $\text{YBa}_2\text{Cu}_3\text{O}_{6.92}$, the result in Fig. 2b shows that $I_{\text{odd}}^{\text{S}}(E) = I_{\text{even}}^{\text{S}}(E) = 5$ for $E = 40$ meV. By substituting $E = 40$ meV and $E_g = 32$ meV into Eqs. 4 and 5, we find $I_{\text{odd}}^{\text{S}}(E) = I_{\text{even}}^{\text{S}}(E) = 5$, in quantitative agreement with the experimental result. For the

overdoped $\text{YBa}_2\text{Cu}_3\text{O}_{6.97}$, the neutron data show that $I_{\text{odd}}^{\text{S}}(E) = I_{\text{even}}^{\text{S}}(E) \approx 10$ for $E = 37$ meV (Ref. [3]). Substituting $E = 37$ meV and $E_g = 33$ meV (Ref. [3]) into Eqs. 4 and 5 yields $I_{\text{odd}}^{\text{S}}(E) = I_{\text{even}}^{\text{S}}(E) = 9.5$, in excellent agreement with the experimental result (≈ 10).

For the optimally doped $\text{YBa}_2\text{Cu}_3\text{O}_{6.92}$, we can also deduce the value of $I_{\text{even}}^{\text{S}}(E_r)/I_{\text{even}}^{\text{N}}(E_r)$ using the measured $I_{\text{odd}}^{\text{S}}(E_r)/I_{\text{odd}}^{\text{N}}(E_r) = 3.6$ and $I_{\text{odd}}^{\text{S}}(E_r) = I_{\text{even}}^{\text{S}}(E_r) = 5$, and the inferred $I_{\text{odd}}^{\text{N}}(E_r) = I_{\text{even}}^{\text{N}}(E_r) \approx 1$ (see above discussion). From the measured $I_{\text{odd}}^{\text{S}}(E_r) = I_{\text{even}}^{\text{S}}(E_r) = 5$, we have $I_{\text{even}}^{\text{S}}(E_r) = 0.2 I_{\text{odd}}^{\text{S}}(E_r)$ and thus $I_{\text{even}}^{\text{S}}(E_r)/I_{\text{even}}^{\text{N}}(E_r) = 0.2 I_{\text{odd}}^{\text{S}}(E_r)/I_{\text{odd}}^{\text{N}}(E_r) = 0.72$. This value is very close to that measured for the single-layer Tl-2201 (0.87). These results consistently suggest that the intralayer neutron intensity at E_r in the superconducting state is slightly lower than that in the normal state. This unique and important feature we have identified definitively rules out d-wave order parameter symmetry because d-wave symmetry predicts that $I_{\text{even}}^{\text{S}}(E_r) = I_{\text{even}}^{\text{N}}(E_r) \gg 1$ for bilayer compounds and $I^{\text{S}}(E_r) = I^{\text{N}}(E_r) \gg 1$ for single-layer compounds.

From Eqs. 1 and 2, it is also easy to calculate E_g and E_r if one knows the gap function (Δ) and the κ value. From the measured Fermi surface, one can readily determine κ . For example, we find $\kappa = 18.4$ for a slightly underdoped BSCCO from Fig. 4. For optimally doped cuprates, we get $\kappa \approx 16.0$. If we would use an isotropic

TABLE I. Comparison of experiments with extended s-wave, d-wave, and isotropic s-wave models, the order parameters are assumed to have opposite signs in the bonding and antibonding electron bands formed within the Cu_2O_4 bilayers. Here DA = definitive agreement, A = agreement, QA = qualitative agreement, PA = possible agreement, D = disagreement and DD = definitive disagreement.

INS data	extended s-wave	d-wave	isotropic s-wave
Feature (a): $I^{\text{S}}(E_r)/I^{\text{N}}(E_r) = 3.6$ for YBCO	DA	DA	DA
Feature (c): $I_{\text{odd}}^{\text{S}}(E_r) = I_{\text{even}}^{\text{S}}(E_r) = 5$ for YBCO	DA	DD	DA
Feature (e): $I^{\text{S}}(E_r)/I^{\text{N}}(E_r) < 1$ for Tl-2201	DA	DD	DA
The magnitudes of E_r and E_g	DA	DD	DD
Spin gap in $\text{La}_{2-x}\text{Sr}_x\text{CuO}_4$	DA	DD	DD
Other data	extended s-wave	d-wave	isotropic s-wave
Penetration depth	DA	QA	DD
Thermal conductivity	DA	QA	DD
Specific heat	DA	QA	DD
Nonlinear Meissner effect	DA	QA	DD
ARPES (underdoped)	A	A	DD
ARPES (overdoped)	DA	DD	DD
Quasiparticle tunneling (underdoped)	PA	PA	DD
Quasiparticle tunneling (overdoped)	DA	DD	DD
Raman scattering (underdoped)	PA	PA	DD
Raman scattering (overdoped)	DA	DD	PA
NMR/NQR	A	A	DD
Andreev reflection	A	PA	DD
Pb/c-axis YBCO Josephson junction	A	D	A
c-axis BSCCO twist Josephson junction	DA	DD	PA
Corner SQUID/Josephson junction	PA	PA	PA
Tricrystal/Tetracrystal Josephson junctions	PA	PA	PA

s-wave gap function $\Delta(\mathbf{k}) = 28 \text{ m eV}$ for a slightly overdoped YBCO, we would have $E_g = 56 \text{ m eV}$ and $E_x > 56 \text{ m eV}$, which are far larger than the measured $E_g = 33 \text{ m eV}$ and $E_x = 40 \text{ m eV}$ (Ref. [3]). If we would use a d-wave gap function $\Delta(\mathbf{k}) = 28 \cos 2\theta \text{ m eV}$, we would have $E_g = 47.5 \text{ m eV}$ and $E_x > 47.5 \text{ m eV}$, which are also far larger than the measured values. These quantitative comparisons constitute another definitive reason to rule out both d-wave and isotropic s-wave symmetries.

Alternatively, an extended s-wave with eight line nodes (A_{1g} symmetry) is in quantitative agreement with two-thirds of the experiments that were designed to test the order-parameter symmetry for hole-doped cuprates [14]. The remaining one-third (e.g., tricrystal grain-boundary Josephson junction experiments) are explained qualitatively by Zhao [14] and by Brandow [15]. In Table 1, we compare nearly all the experiments used to test the OP symmetry with the extended s-wave, d-wave, and isotropic s-wave models. In both extended s-wave and isotropic s-wave models, the order parameters are assumed to have opposite signs in the bonding and antibonding electron bands formed within the Cu_2O_4 bilayers [16]. The detailed comparisons with other experiments are made in Ref. [14]. From Table 1, one can see that the neutron data alone provide a definitive answer to the intrinsic, bulk OP symmetry because INS is a bulk, phase and angle sensitive technique. Other bulk and non-phase sensitive experiments provide complementary support to the present conclusions. The phase and surface sensitive experiments can at most tell that, at the surface, there is a d-wave component that could be slightly smaller or far larger than an extended s-wave component. These experiments cannot definitively determine the intrinsic bulk OP symmetry especially when the surfaces are strongly degraded and the OP is dramatically reduced at surfaces.

For a slightly overdoped YBCO, more than six independent experiments consistently suggest that [14] the gap function is $\Delta(\mathbf{k}) = 24.5(\cos 4\theta + 0.225) \text{ m eV}$. Substituting $\theta_x = 16^\circ$ into the gap function, we get $\Delta(\theta_x) = 16.3 \text{ m eV}$ and thus $E_g = 32.6 \text{ m eV}$, in quantitative agreement with the measured one (32–33 m eV).

In our model, the position of the extended saddle point along the θ_x direction is located at $E_x - E_g = 2$ in the superconducting state (see Eqs. 1 and 2). For optimally doped YBCO with $E_x = 41 \text{ m eV}$ and $E_g = 32 \text{ m eV}$, we find that the saddle point in the superconducting state is located at an energy of 25 m eV below the Fermi level. This is in agreement with the ARPES studies [28] which suggest that the Fermi level in the superconducting state for optimally doped cuprates is 30 m eV above the extended saddle points that have the same energy over a large momentum space [23]. Further, electronic Raman scattering spectra in $\text{YBa}_2\text{Cu}_4\text{O}_8$ have been used to determine the energy of the extended saddle points more accurately [29]. At 10 K (well below T_c), the energy of

the extended saddle points is found to be 24.3 m eV below the Fermi level, in excellent agreement with the result predicted by our model from the INS data ($\sim 25 \text{ m eV}$).

We have identified the unique and important feature (e): $I^S(E_x)/I^N(E_x) < 1$ for the intralayer magnetic scattering. This feature unambiguously rules out the d-wave OP symmetry and the role of magnetic excitations in superconductivity. This feature alone can also disprove all the theoretical models based on d-wave pairing and/or the antiferromagnetic electron correlation. The unambiguous determination of the intrinsic extended s-wave pairing symmetry for hole-doped cuprates provides strong support for a theoretical model proposed early on by Littlewood and co-workers [17]. Based on a three-band Hubbard model, they showed that undamped charge fluctuations between Cu and O could induce electron pairing with A_{1g} (extended s-wave) symmetry [17]. The energy of the charge fluctuations is about 2 eV. A recent exact calculation [18] has confirmed this early theoretical model.

Indeed, precise thermal-dielectric reflectance spectra of several cuprate superconductors ($T_c = 105\text{--}120 \text{ K}$) exhibit pronounced features at photon energies of about 2.0 eV (Ref. [30]). These features can be well described within Eliashberg theory with an electron-boson coupling constant λ_{ch} of about 0.40. In order to explain a superconducting transition temperature of 105–120 K, the authors simulated [30] an electron-phonon coupling feature at 50 m eV with the coupling constant λ_{ph} of about 1.0. This Eliashberg model's simulated electron-phonon coupling agrees well with the result obtained from a first-principle calculation for $\text{La}_{1.85}\text{Sr}_{0.15}\text{CuO}_4$ (Ref. [31]).

The contribution of this 2 eV component can be equivalent to a negative Coulomb pseudopotential within Eliashberg theory [32]. One can readily show that the equivalent μ^* for this 2 eV component is about -0.15 for those superconductors with $T_c > 90 \text{ K}$. By using a realistic electron-phonon coupling spectral weight deduced from tunneling spectra and a $\mu^* = -0.15$, a polaronic effect [33] can well explain the negligible isotope effect on T_c observed in optimally doped 90 K superconductors. As proposed by Alexandrov and Mott [34] and confirmed by extensive isotope effect experiments [35], superconductivity for deeply underdoped cuprates arises from the Bose-Einstein condensation of bipolarons (real-space pairs), Thus high-temperature superconductivity in cuprates is due to the combination of strong electron-phonon coupling [35–37] and substantial electron-charge-fluctuation coupling [17,18,30]. The antiferromagnetic spin fluctuations tend to reduce superconductivity for s-wave pairing [38].

Correspondence should be addressed to gzhao2@calstatela.edu

-
- [1] Bourges, P., Sidis, Y., Hennion, B., Villeneuve, R., Collin, G., and Marucco, J.F. Spin dynamics in the high- T_c superconducting system $YBa_2Cu_3O_{6+x}$. *Physica B*, 213-214, 48-53 (1995).
- [2] Fong, H.F., Keimer, B., Anderson, P.W., Reznik, D., Dogan, F., and Aksay, I.A., Phonon and magnetic neutron scattering at 41 meV in $YBa_2Cu_3O_7$. *Phys. Rev. Lett.* 75, 316-319 (1995).
- [3] Bourges, P., Regnault, L.P., Sidis, Y. and Vettier, C. Inelastic-neutron-scattering study of antiferromagnetic fluctuations in $YBa_2Cu_3O_{6.97}$. *Phys. Rev. B* 53, 876-885 (1996).
- [4] Bourges, P. From magnons to the resonance peak: Spin dynamics in high- T_c superconducting cuprates by inelastic neutron scattering The gap Symmetry and Fluctuations in High Temperature Superconductors, Edited by Bok, J., Deutscher, G., Pavuna, D., and Wolf, S.A. (Plenum Press, 1998) p 349-371 (Vol. 371 in NATO ASI series, Physics).
- [5] Bourges, P., Sidis, Y., Fong, H.F., Keimer, B., Regnault, L.P., Bossy, J., Ivanov, A.S., Milius, D.L., and Aksay, I.A. Spin dynamics in high- T_c superconductors. *High Temperature Superconductivity*, Edited by Barnes S.E. et al p207-212 (CP 483 American Institute of Physics, Amsterdam, 1999)
- [6] Dai, P.C., Mook, H.A., Hunt, R.D., and Dogan, F. Evolution of the resonance and incommensurate spin fluctuations in superconducting $YBa_2Cu_3O_{6+x}$. *Phys. Rev. B* 63, 054525-054544 (2001).
- [7] Fong, H.F., Bourges, P., Sidis, Y., Regnault, L.P., Ivanov, A., Guk, G.D., Koshizuka, N., and Keimer, B. Neutron scattering from magnetic excitations in $B_{1/2}Sr_2CaCu_2O_{8+}$. *Nature (London)* 398, 588-591 (1999).
- [8] He, H., Sidis, Y., Bourges, P., Gu, G.D., Ivanov, A., Koshizuka, N., Liang, B., Lin, C.T., Regnault, L.P., Schoenherr, E., and Keimer, B. Resonant spin excitation in an overdoped high temperature superconductor. *Phys. Rev. Lett.* 86, 1610-1613 (2001)
- [9] He, H., Bourges, P., Sidis, Y., Ulrich, C., Regnault, L.P., Pailhes, S., Berzigiarova, N.S., Kolesnikov, N.N., and Keimer, B. Magnetic resonant mode in the single-layer high temperature superconductor $T_{1/2}Ba_2Cu_{6+}$. *Science* 295, 1045-1047 (2002).
- [10] Demler, E., Kohn, H., and Zhang, S.C. π -excitation of the t-J model. *Phys. Rev. B* 58, 5719-5730 (1998).
- [11] Abanov, A. and Chubukov, A.V. A relation between the resonance neutron peak and ARPES data in cuprates. *Phys. Rev. Lett.* 83, 1652 (1999).
- [12] Morr, D.K. and Pines, D., The resonance peak in cuprate superconductors. *Phys. Rev. Lett.* 81, 1086-1089 (1998).
- [13] Brinkmann, J. and Lee, P.A. Slave boson approach to neutron scattering in $YBa_2Cu_3O_{6+y}$ Superconductors. *Phys. Rev. Lett.* 82, 2915 (1999).
- [14] Zhao, G.M. Identification of the bulk pairing symmetry in high-temperature superconductors: Evidence for an extended s-wave with eight line nodes. *Phys. Rev. B* 64, 024503-024512 (2001).
- [15] Brandow, B.H. Arguments and evidence for a node-containing anisotropic s-wave gap form in the cuprate superconductors. *Phys. Rev. B* 65, 054503-054517 (2002).
- [16] Mazin, I.I. and Yakovenko, V.M. Neutron scattering and superconducting order parameter in $YBa_2Cu_3O_7$. *Phys. Rev. Lett.* 75, 4134-4137 (1995).
- [17] Littlewood, P.B., Varma, C.M., and Abrahams, E. Pairing instabilities of extended Hubbard model for Cu-O based superconductors. *Phys. Rev. Lett.* 63, 2602-2605 (1989); Littlewood, P.B. Collective modes and superconductivity in an extended Hubbard model for copper oxide superconductors. *Phys. Rev. B* 42, 10075-10089 (1990).
- [18] Gulacsi, M. and Chan, R. High-temperature superconductivity: The attractive U_p regime. *J. Supercond.* 14, 651-658 (2001).
- [19] Bardeen, J., Cooper, L.N. and Schrieffer, J.R. Theory of Superconductivity. *Phys. Rev.* 108, 1175-1204 (1957).
- [20] Alexandrov, A.S. and Mott, N.F. Bipolarons. *Rep. Prog. Phys.* 57, 1197-1290 (1994).
- [21] McElroy, K., Simmonds, R.W., Homann, J.E., Lee, D.H., Orenstein, J., Eisaki, H., Uchida, S., and Davis, J.C. Relating atomic-scale electronic phenomena to wave-like quasiparticle states in superconducting $B_{1/2}Sr_2CaCu_2O_{8+}$. *Nature* 422, 592-596 (2003).
- [22] White, P.J., Shen, Z.-X., Kim, C., Harris, J.M., Loeser, A.G., Fournier, P., and Kapitulnik, A. Rapid suppression of the superconducting gap in overdoped $B_{1/2}Sr_2CaCu_2O_{8+}$. *Phys. Rev. B* 54, R15 669-15672 (1996).
- [23] Dessau, D.S., Shen, Z.-X., King, D.M., Marshall, D.S., Lombardo, L.W., Dickinson, P.H., Loeser, A.G., DiCarlo, J., Park, C.H., and Kapitulnik, A., and Spicer, W.E. Key features in the measured band structure of $B_{1/2}Sr_2CaCu_2O_{8+}$: Flat bands at E_F and Fermi surface nesting. *Phys. Rev. Lett.* 71, 2781-2784 (1993).
- [24] Curro, N.J., Imai, T., Slichter, C.P., and Dabrowski, B. High-temperature $^{63}Cu(2)$ nuclear quadrupole and magnetic resonance measurements of $YBa_2Cu_4O_8$. *Phys. Rev. B* 56, 877 (1997).
- [25] Ubbens, M.U. and Lee, P.A. Spin gap formation in bilayer cuprates due to enhanced interlayer pairing. *Phys. Rev. B* 50, 438-451 (1994).
- [26] Schrieffer, J.R., *Theory of Superconductivity*, (Frontiers in Physics (20), Addison Wesley, 1988).
- [27] Fong, H.F., Bourges, P., Sidis, Y., Regnault, L.P., Bossy, J., Ivanov, A., Milius, D.L., Aksay, I.A., and Keimer, B. Spin susceptibility in underdoped $YBa_2Cu_3O_{6+x}$. *Phys. Rev. B* 61, 14773-14786 (2000).
- [28] King, D.M., Shen, Z.-X., Dessau, D.S., Marshall, D.S., Park, C.H., Spicer, W.E., Peng, J.L., Li, Z.Y., and Greene, R.L. Observation of a saddle-point singularity in $B_{1/2}(Sr_{0.97}P_{0.03})CuO_{6+}$ and its implications for normal and superconducting state properties. *Phys. Rev. Lett.* 73, 3298-3301 (1994).
- [29] Shernan, E.Ya. and Misochko, O.V. Extended Van Hove singularity in electronic Raman scattering in $YBa_2Cu_4O_8$. *Phys. Rev. B* 59, 195-198 (1999).
- [30] Holcomb, M.J., Perry, C.L., Collman, J.P., and Little,

- W. A. Thermally-difference reflectance spectroscopy of the high-temperature cuprate superconductors. *Phys. Rev. B* 53, 6734-6751 (1996).
- [31] Krakauer, H., Pickett, W. E., and Cohen, R. E. Large calculated electron-phonon interactions in $\text{La}_{2-x}\text{Sr}_x\text{CuO}_4$. *Phys. Rev. B* 47, 1002-1015 (1993).
- [32] Carbotte, J. P. Properties of boson-exchange superconductors. *Rev. Mod. Phys.* 62, 1027-1157 (1990).
- [33] Zhao, G. M., Kirtikar, V., and Morris, D. E. Isotope effects and possible pairing mechanism in optimally doped cuprate superconductors. *Phys. Rev. B* 64, R220506-220509 (2001).
- [34] Alexandrov, A. S. and Mott, N. F., *Polarons and Bipolarons* (World Scientific, Singapore, 1995).
- [35] Zhao, G. M., Hunt, M. B., Keller, H., and Muller, K. A. Evidence for polaronic supercarriers in the copper oxide superconductors $\text{La}_{2-x}\text{Sr}_x\text{CuO}_4$. *Nature* (London) 385, 236-238 (1997); Zhao, G. M., Keller, H. and Conder, K. Unconventional isotope effects in the high-temperature cuprate superconductors. *J. Phys.: Condens. Matter* 13, R569-R587 (2001).
- [36] McQueeney, R. J., Petrov, Y., Egami, T., Yethiraj, M., Shirane, G., and Endoh, Y. Anomalous dispersion of LO phonons in $\text{La}_{1.85}\text{Sr}_{0.15}\text{CuO}_4$ at low temperatures. *Phys. Rev. Lett.* 82, 628-631 (1999).
- [37] Lanzara, A. et al. Evidence for ubiquitous strong electron-phonon coupling in high-temperature superconductors. *Nature* 412, 510-514 (2001).
- [38] Wempe, S. and Tewordt, S. Photoemission intensity and density of states in the superconducting state of $\text{Bi}_2\text{Sr}_2\text{CaCu}_2\text{O}_8$. *Phys. Rev. B* 46, 12061-12063 (1992).